Physics and Chemistry of Minerals (2023) 50:21
https://doi.org/10.1007/s00269-023-01246-5

ORIGINAL PAPER

High-temperature behavior of quartz-in-garnet system revealed by in situ Raman spectroscopy

Marta Morana[1] · Ross J. Angel[2] · Matteo Alvaro[3] · Boriana Mihailova[4]

Received: 4 April 2023 / Accepted: 23 June 2023 / Published online: 7 July 2023

Abstract

Quartz is one of the most abundant minerals in the Earth crust and therefore quartz inclusions in garnet are of great interest for elastic geobarometry, an approach that exploits the elastic properties of the mineral pair to back-calculate the conditions of inclusion entrapment. However, the high-temperature behavior of quartz inclusions close to the α–β transition boundary has not been studied experimentally. We have therefore performed in situ high-temperature Raman spectroscopy on a quartz-in-garnet system up to 1000 K, and have also collected an improved reference data set for the temperature dependence of the Raman scattering of free quartz. Our results show that the α-to-β phase transition is hindered by the stress imposed by the host on the quartz inclusion, resulting in a thermosalient effect of the whole host-inclusion system or a mechanical cracking of the host mineral.

Keywords Host-inclusion system · Geobarometry · Phase transition · Thermoelastic properties

Introduction

Quartz is one of the most studied minerals due to its natural abundance, rich polymorphism, and technologically important physical properties (e.g. Ballato 2008; Curie and Curie 1880; Jorgensen 1978; Glinnemann et al 1992; Hazen et al 1989; Wang et al 2015; Scheidl et al 2016). The temperature-induced displacive α–β phase transition of quartz has drawn much attention over time, including a lively debate on its nature (Salje et al 1992; Dove et al 1999), and it was one of the first phase transitions characterized by Raman spectroscopy (Raman and Nedungadi 1940). Both phases are chiral (Donnay and Le Page 1978), and the transition from the high-temperature β-phase ($P6_222$ or $P6_422$) to the low-temperature α-phase ($P3_121$ or $P3_221$) consists of a slight rotation of the SiO_4 tetrahedra around their two-fold axis, with the rotation angle ϕ taken as a microscopic order parameter (Grimm and Dorner 1975). The critical phase-transition temperature T_c is ~847 K at atmospheric pressure and increases with pressure (e.g. Shen et al 1993). Recently, quartz inclusions have been employed in elastic geobarometry, a methodology that allows the pressure and temperature conditions of inclusion entrapment to be determined from the difference in thermoelastic and elastic properties between the host and the inclusion (e.g. Bonazzi et al 2019; Alvaro et al 2020). Raman spectroscopy is often the technique of choice to measure the residual pressure in the inclusion, as a straight-forward method with a spatial resolution down to a few microns (Campomenosi et al 2018; Mazzucchelli et al 2018; Murri et al 2018; Bonazzi et al 2019). The inclusion pressure can be determined from the difference in the Raman peak positions of an inclusion from those of a free crystal through a hydrostatic calibration (Schmidt and Ziemann 2000; Morana et al 2020) or by using the recently developed phonon-mode

✉ Marta Morana
marta.morana@unifi.it

Ross J. Angel
ross.angel@igg.cnr.it

Matteo Alvaro
matteo.alvaro@unipv.it

Boriana Mihailova
boriana.mihailova@uni-hamburg.de

[1] Department of Earth Sciences, University of Florence, Via G. La Pira 4, 50121 Florence, Italy

[2] Istituto di Geoscienze e Georisorse, Consiglio Nazionale delle Ricerche, Via G. Gradenigo 6, 35131 Padua, Italy

[3] Department of Earth and Environmental Sciences, University of Pavia, Via A. Ferrata, 1, 27100 Pavia, Italy

[4] Department of Earth Sciences, Universität Hamburg, Grindelallee 48, 27100 Hamburg, Germany

Grüneisen-tensor approach (Murri et al 2018; Angel et al 2019). Mineral inclusions also provide the opportunity to study the behavior of minerals under non-hydrostatic stress conditions, because any elastic anisotropic crystal entrapped in another solid develops a deviatoric stress state (Angel et al 2019). In situ temperature-dependent studies have also been proposed as a tool to explore the thermoelastic properties of host-inclusions system and to test the applicability of elastic geobarometry (Campomenosi et al 2023; Ashley et al 2016). For example, Campomenosi et al (2023) showed that zircon inclusions in garnet might experience resetting, depending on the exhumation path of the host rock, thus providing a further constraint on the *P-T* history of metamorphic rocks. Although the elastic and thermoelastic properties of quartz considerably change across the α–β phase transition (Carpenter et al 1998; Angel et al 2017), little is known about the behavior of quartz inclusions at elevated temperatures around T_c. To fill this gap of knowledge, here we report our results from in situ high-temperature Raman spectroscopy on a quartz-in-garnet (QuiG) system, together with a reexamination of the temperature dependence of the Raman scattering of free quartz. We show that stress in the quartz inclusion suppresses the α-to-β phase transition. Instead, the energy accumulated in the inclusion near the anticipated T_c is anisotropically released to the surrounding host, leading to a thermosalient effect of the whole QuiG sample or a mechanical cracking of the host garnet. In addition, we provide an improved wavenumber-vs-temperature reference dependence for the interpretation of the inclusion data.

Materials and methods

Oriented (010)- and (001)-cuts of a gem-quality quartz, provided by the Mineralogical Museum, Universität Hamburg, were used as a reference free quartz. A garnet with a quartz inclusion was extracted from a polished section from the microdiamond-bearing garnet-kyanite gneiss in the Blåhø nappe, Fjørtoft, Nordøyane archipelago, Norway (Dobrzhinetskaya et al 1995; Larsen et al 1998; Liu and Massonne 2019). The overall dimensions of the QuiG-sample were 400 × 40 × 300 μm. The host mineral is garnet, with composition pyrope: 0.33, almandine: 0.60, grossular: 0.05, spessartine: 0.02 (Gilio et al 2022). It contained a large quartz inclusion (60 × 40 μm), two smaller zircon inclusions, approximately 80 and 120 μm distant from the quartz inclusion, and rutile exsolution needles. Spectra were acquired at the center of the inclusion, in the host close to the host-inclusion boundary and away from the inclusion. The spectra collected from the host away from the inclusion were subtracted from the inclusion spectra, since the peak positions of the garnet host were the same throughout the sample.

Polarized Raman spectra were collected with a Horiba Jobin-Yvon T64000 triple-monochromator system equipped with a Symphony LN_2-cooled CCD detector, an Olympus BH41 microscope, and a Coherent Ar^+ laser. The measurements were performed in backscattering geometry, with a 50× super-long working distance objective and an excitation wavelength of 514.532 nm. The spectrometer was calibrated to the T_{2g} mode at 520.5 cm^{-1} of a silicon wafer. The spectral resolution was approximately 2 cm^{-1}, while the instrumental precision in the peak positions was 0.35 cm^{-1}. The data collection was conducted on heating from room temperature with a heating rate of 50 K min^{-1} between measurements, in a Linkam TS1200 stage equipped with a Linkam T95 controller. The sample was kept for 5 min at the desired experimental temperature before the data collection was started. The acquisition time was set to obtain a satisfactory signal-to-noise ratio, and thus the spectra were collected for 30 s averaging over a minimum of 5 accumulations in the wavenumber range 15–1615 cm^{-1}. To account for the Bose-Einstein occupation factor, the intensity of the measured spectra was temperature-corrected using the relation $I = I_{\text{measured}}/[(\exp^{\hbar\omega/k_BT} - 1)^{-1} + 1]$, where $\hbar$, ω, k_B, and T are the reduced Planck constant, phonon wavenumber, Boltzmann constant, and temperature, respectively. The spectra were then normalized to the acquisition time. Pseudo-Voigt functions ($PV = qL + (1 - q)G$, where L and G are Lorentzian and Gaussian peak-shape functions) were used to fit the spectra and determine the Raman peak positions ω, full widths at half maximum (FWHMs), and integrated intensities I. The A_1 mode at 465 cm^{-1} shows a pronounced asymmetry upon increasing temperature, resulting from multi-phonon excitation (Schmidt and Ziemann 2000), which cannot be taken into account by a single Pseudo-Voigt function. As consequence, an additional peak was introduced in the fitting model at elevated temperatures, following the fitting procedure described in Murri et al (2019).

Results and discussion

Group-theory analysis and high-temperature Raman scattering of free quartz

The Brillouin-zone-center optical phonon modes in α-quartz are $\Gamma_{opt}^{\alpha-Q} = 4A_1(R)+4A_2(IR)+8E(R,IR)$, while those in β-quartz are $\Gamma_{opt}^{\beta-Q} = A_1(R)+2A_2(IR)+2B_2(ina)+3B_1(ina) + 4E_1(R,IR)+4E_2(R)$, where "R", "IR", and "ina" designate Raman-active, IR-active and inactive modes, respectively. The E modes in α-quartz as well as the E_1 modes in β-quartz are simultaneously Raman- and IR-active and thus show transverse optic (TO) and longitudinal optic (LO) components. The symmetry relationships between

irreducible representations for the two phases is shown in the correlation diagram in Table S1 (Bates and Quist 1972). The Raman-active phonon modes selected for this study in the two phases as well as their peak positions observed correspondingly below and above the phase transition are given in Table 1.

Figure 1a shows the Raman spectra of free quartz at selected temperatures, indicating that the 465 cm^{-1} mode is not the only A_1 that persists in the β-phase, as would be expected from group factor analysis. In fact, the A_1 mode around 207 cm^{-1} is still present after the α-β transition. This mode is the most sensitive to temperature and has often been considered as the soft mode driving the phase transition. However, for a soft-mode-driven displacive phase transition, the phonon wavenumber of the soft mode should decrease to zero as the transition temperature is reached (Cochran 1960; Ginzburg 1960), which is not the case for A_1 ~207 cm^{-1}. It was proposed that the true soft-mode excitation triggering the α-β phase transition is a two-phonon excitation of A_1 symmetry, which at room temperature appears around 147 cm^{-1} (Scott 1968, 1974). As can be seen in Fig. 1b, this two-phonon excitation is strongly enhanced when approaching T_c and its wavenumber and FWHM show typical soft-mode behavior (Fig. 2). The softening of the fundamental A_1 ~ 207 cm^{-1} thus results from its interaction with the true soft-mode excitation near 147 cm^{-1} (Scott 1968). These two spectral features are mixed via Fermi resonance, and above T_c the parent A_1 ~207 cm^{-1} mode is preserved (see Fig. 1) because of its predominantly second-order Raman-activity (Scott 1968). The temperature dependence of the peak positions and FWHM for the 128, 207, 355 and

Table 1 Peak positions of selected Raman active modes (cm^{-1}) for α- and β-quartz

α-quartz (D_3)				β-quartz (D_6)		
Symmetry	Activity	ω_{300K}	ω_{840K}	Symmetry	Activity	ω_{870K}
E(TO)	*xx*, *yy*, *yz*, *xy*, *xz*	128.24 (3)[1]	106.2 (9)	E_1(LO)	*yz*, *xz*	97.7 (1)[2]
A_1	*xx*, *yy*, *zz*	207.27 (5)	174.9 (5)			168.0 (5)[3]
E(TO)	*xx*, *yy*, *yz*, *xy*, *xz*	263.5 (9)	252 (3)	E_2	*xx*, *yy*, *xy*	249 (1)
A_1	*xx*, *yy*, *zz*	355.12 (5)	353.9 (4)			
E(TO)	*xx*, *yy*, *yz*, *xy*, *xz*	393.89 (9)	397.6 (3)	E_2	*xx*, *yy*, *xy*	402.6 (5)
A_1	*xx*, *yy*, *zz*	464.775 (6)	457.83 (4)	A_1	*xx*, *yy*, *zz*	458.87 (3)
E(TO)	*xx*, *yy*, *yz*, *xy*, *xz*	696.0 (2)	684.5(9)	E_2	*xx*, *yy*, *xy*	684 (1)
E(TO)	*xx*, *yy*, *yz*, *xy*, *xz*	1161.0 (1)	1161.9 (4)	E_2	*xx*, *yy*, *xy*	1168.4 (4)

Reported uncertainties are from spectral fitting

[1]Observed in scattering geometry $\bar{z}$(xx)z

[2]Observed in scattering geometry $\bar{y}$(xz)y

[3]Anomalous Raman activity stemming from the parent fundamental A_1 mode, see text for details

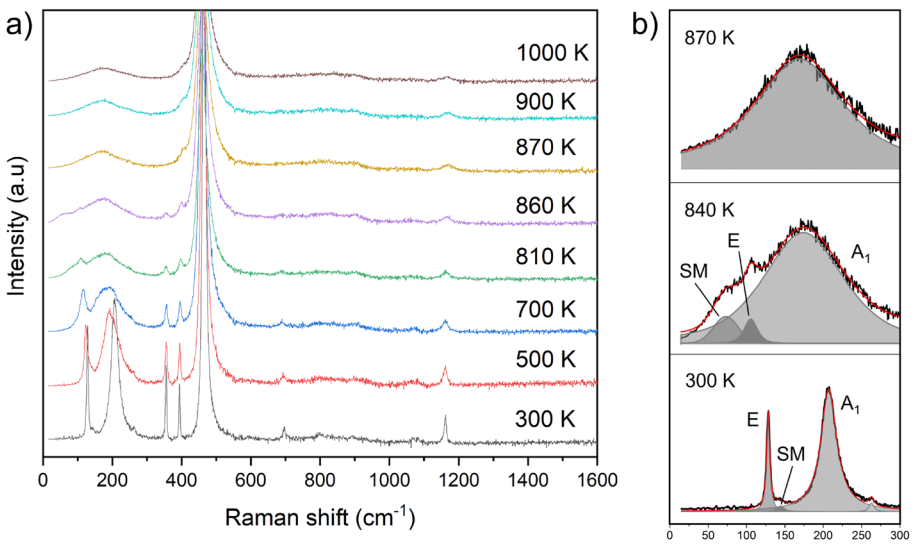

Fig. 1 **a** Selected spectra of free quartz upon increasing temperature in the $\bar{z}(xx)z$ scattering geometry. **b** Close-ups of the region below 300 cm^{-1} are showed at 300 K and at T immediately before and after the phase transition with the fitted peak functions. The enhancement of the soft mode near 147 cm^{-1} upon heating and its disappearance above T_c are clearly apparent

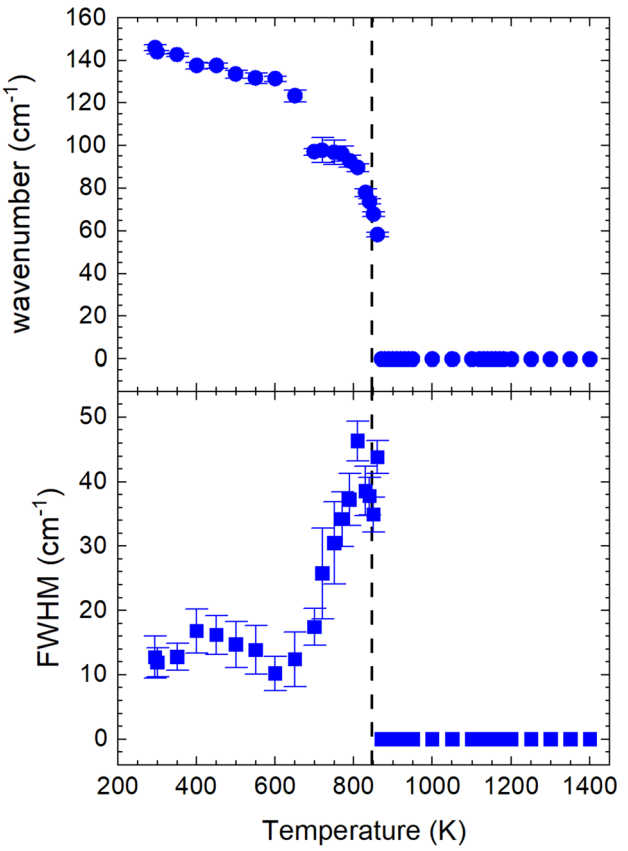

Fig. 2 Temperature dependence of the peak position and FWHM of the two-phonon excitation SM~147 cm^{-1}, which is the true soft-mode excitation triggering the α-to-β phase transition (Scott 1968, 1974). The dashed line indicates the α-β transition temperature at ambient pressure

465 cm^{-1} modes and the 147 cm^{-1} two-phonon band are reported in tables S2 and S3.

Residual pressures of the quartz inclusion

The residual pressure of the quartz inclusion P_{inc} was determined using three different methods: (i) calculating the strains from the wavenumber shifts and the quartz elastic tensor, as described in Bonazzi et al (2019); (ii) using the *EntraPT* software (Mazzucchelli et al 2021); (iii) applying a wavenumber shift versus pressure equation obtained from high pressure experiments (Morana et al 2020). Within uncertainties, all methods point to a room-temperature P_{inc} ~0.30 GPa, see SI for details. From this value of P_{inc}, the pressure of entrapment P_{trap} (1.353, 1.371 and 1.290 GPa for almandine, grossular and pyrope, respectively) was calculated at a temperature of entrapment T_{trap} of 1050 K, which was previously estimated for this locality by Gilio et al (2022); detailed information about the calculation is provided in the SI.

The temperature dependencies of the wavenumber ω and FWHM Γ for selected phonon modes in QuiG and in a free quartz are compared in Fig. 3, to reveal the effect of the garnet host on the quartz-inclusion strain with the temperature increase. Except for the A_1 mode at 355 $^{-1}$, which even in a free quartz is insensitive to temperature changes as well as to a pressure increase up to ~2.0 GPa (Morana et al 2020), for all Raman modes $\omega_{QuiG} > \omega_{quartz}$ at the same temperature. This confirms that the inclusion remains under pressure over the entire temperature range of the measurements. Besides, in the temperature range of α-quartz stability, the slope of $\omega(T)$ is steeper for free quartz than for QuiG. For example, the linear fits to data points below 600 K provide that $\omega(T)/dT$ for free quartz vs QuiG is −0.0551(4) vs −0.035(2) for A_1(207) and −0.0144(2) vs −0.0120(8) for A_1(465). This emphasizes that the confinement effect of the host on the inclusion increases at elevated temperatures, because of the differences in the volume thermal expansion of garnet and quartz [at room temperature α_V^{pyr}=2.256 (5) x 10^{-5} K^{-1}, α_V^{alm}=1.957 (5) x 10^{-5} K^{-1}(Angel et al 2022), α_V^{qtz}=4.31 (4) × 10^{-5} K^{-1} (Ackermann and Sorrell 1974)]. In particular, α_V^{quartz} tends to infinite values at temperatures on the approach to the α –β phase transition, with the unit-cell volume increasing by about 5% between room temperature and T_c (Carpenter et al 1998; Angel et al 2017), and then becomes negative in the β-phase (Heine et al 1999; Welche et al 1998), whereas the thermal expansion coefficients of garnets increase only slightly (Angel et al 2022). When approaching the transition temperature expected at ambient pressure, T_c=847 K, the A_1 (207) and A_1(465) in free quartz show typical behavior of hard phonon modes coupled with the soft-mode excitation (Bismayer 1990): in the vicinity of the phase transition $\omega(T)$ exhibits a minimum, while $\Gamma(T)$ becomes larger due to the reorganization of the structure from the α to the β phase. In contrast, $\omega(T)$ for the quartz inclusion do not show a clear minimum and above 847 K the data points are clustered around a constant value. Moreover, $\Gamma(T)$ shows only a trivial increase upon heating [due to increasing phonon decay (Kuzmany 2009)], without being in excess. Besides, the E(128) and A_1(355) persist above 847 K (see Fig. 3), as all resolved Raman peaks typical of α-quartz do (see Fig. 4 and Table S9). All these observations show that a phase transition does not occur in QuiG up to 1000 K.

The calculated entrapment conditions P_{trap} (1.353, 1.371 and 1.290 GPa for almandine, grossular and pyrope, respectively) at 1050 K were then used to determine the P_{inc} at different temperature through the equations of state of the host (Angel et al 2022), and the inclusion (Angel et al 2017), under the assumption of hydrostatic conditions in the inclusion (see section 2.2 in ESM1 for further details). The calculation was performed for almandine and pyrope, the

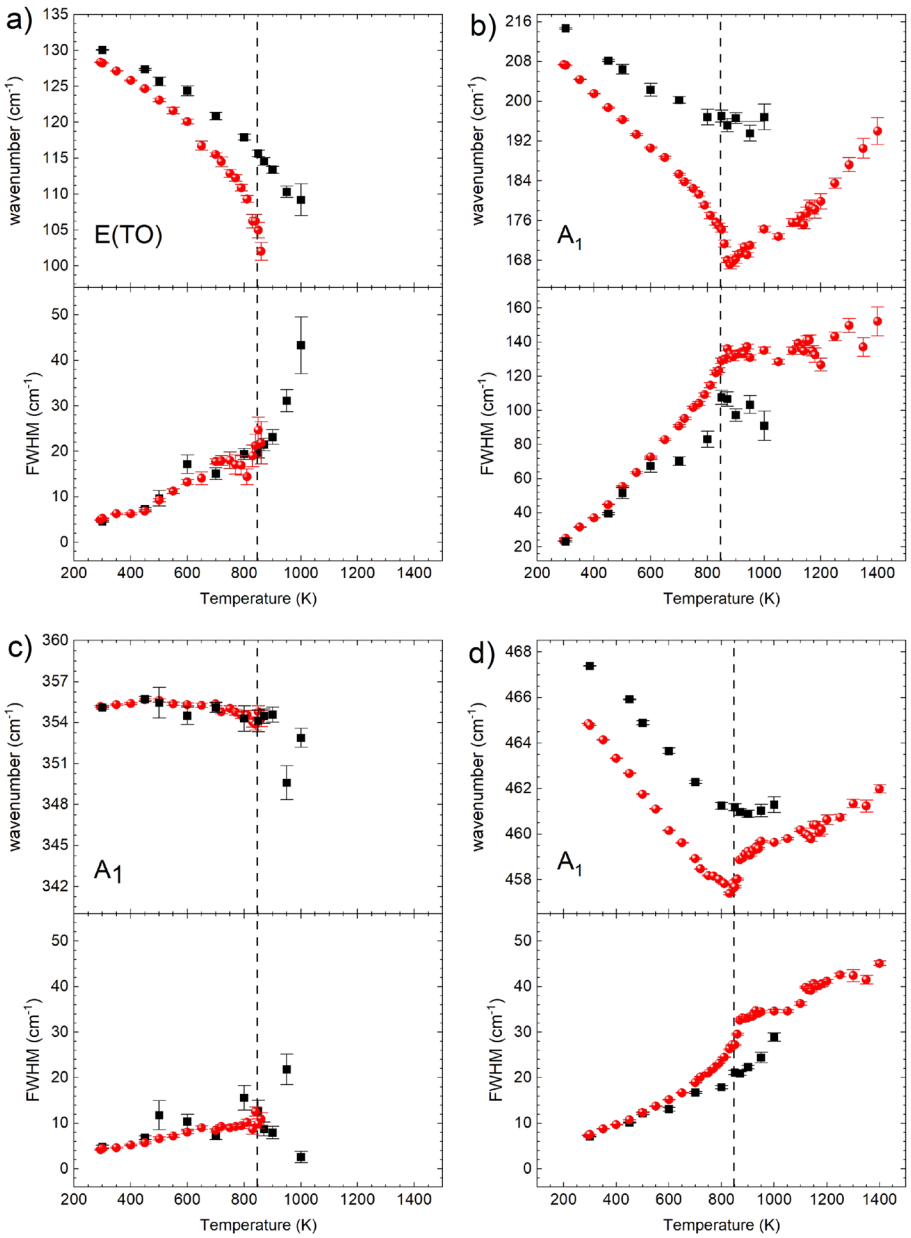

Fig. 3 Temperature dependence of the peak positions and FWHMs of selected modes for a free (red) and trapped quartz (black) for the 128 cm^{-1} (**a**), 207 cm^{-1} (**b**), 355 cm^{-1} (**c**) and 465 cm^{-1} (**d**) modes in the $\bar{z}(xx)z$ scattering geometry. Dashed lines indicate the α-β transition temperature at ambient pressure

two most abundant endmember components in the sample, while grossular gives an intermediate results, as expected from its thermoelastic properties (Angel et al 2022). From this calculation, the α–β transition is predicted to occur in the inclusion at 1171 and 1162 K for almandine and pyrope, respectively (Fig. 5), which is consistent with the expected increase in the transition temperature from T_c=847 K at atmospheric pressure due to a pressure of 0.3 GPa.

To have a further insight into the inclusion stress state, we have compared the P_{inc} back-calculated from the inclusion entrapment conditions with the P_{inc} obtained by applying a hydrostatic calibration (Morana et al 2020), to the $\Delta\omega$ calculated as the difference between the Raman peak position in the free and in the trapped quartz at the same temperature (solid symbols in Fig. 5). Below 600 K, the two sets of P_{inc} are the same within uncertainties, indicating that the QuiG system is behaving elastically. Above this temperature, from ca 600 K to ca 850 K, the agreement is worse, in particular for the modes at 128 and 207 cm^{-1}, which are both more sensitive to pressure and temperature changes than the mode at 465 cm^{-1} (Morana et al 2020; Murri et al 2019). In fact, as shown in Figs. 1 and 4 and discussed in the previous section, these two modes undergo large variations upon heating. This is especially true for the mode at 207 cm^{-1}, since it is involved in a complex interaction with the two-phonon band of A_1 symmetry, which also shows a huge change in the FWHM starting from 600 K (Fig. 2). It is also worth noting that

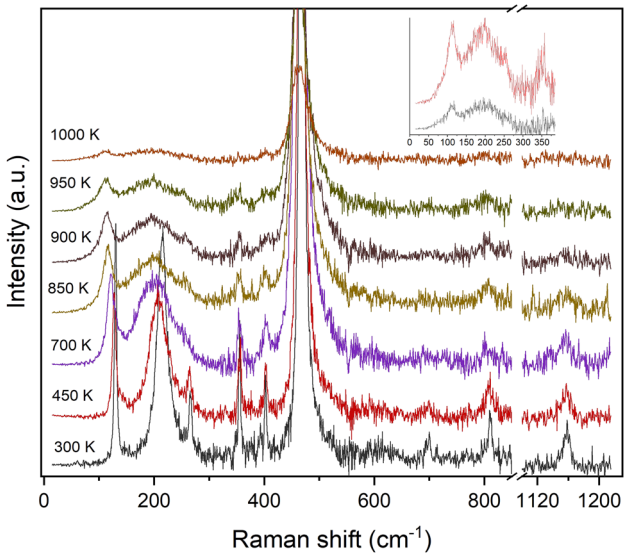

Fig. 4 Example Raman spectra from the quartz inclusion at various temperatures obtained after subtracting the host spectra. The inset contains a close-up of the region below 350 cm^{-1}, showing that the E(128) and A_1(355) modes persist above 847 K

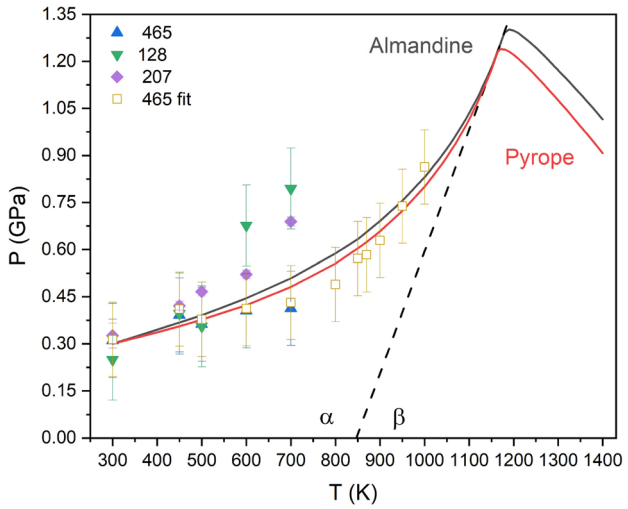

Fig. 5 Expected pressure evolution of a quartz inclusion calculated with almandine and pyrope as the host, plotted as lines. Solid symbols are calculated with the hydrostatic calibration (Morana et al 2020) for the modes at 128, 207 and 465 cm^{-1} up to 700 K. Open symbols are the pressures calculated applying the hydrostatic calibration to a linear fit of the free quartz data. The dashed line represents the α–β phase transition boundary

different modes provide different pressure values. This is expected because the quartz inclusion, being an anisotropic mineral trapped inside a cubic host, is not under hydrostatic conditions and thus its stress state cannot be described by a single pressure value (Anzolini et al 2018; Murri et al 2018). Other explanations for this deviation, such as the dependence of $(d\omega/dT)$ upon pressure or the difference in the host composition, can be excluded. In fact, Schmidt and Ziemann (2000) showed that at least the 465 cm^{-1} mode has a constant isotherm slope up to 1.1 GPa. The composition of the garnet is not a reason for the discrepancy, since, as shown in Fig. 5, the differences in calculated P_{inc} for different garnet endmembers are small. This calculation of P_{inc} cannot be applied at higher temperature, since the free quartz data show the typical trend due to the phase transition that is not present in the inclusion data, as already discussed (Fig. 4). In order to exclude the transition effects, for the 465 cm^{-1} mode, $\Delta\omega$ was calculated as the difference between the peak positions of the inclusion with respect to the position obtained from a linear fit to the free quartz data up to 600 K [$\Delta\omega_{465}$ = 4.5(1)−0.015(3)T], and this $\Delta\omega$ was then converted to a pressure. The resulting P_{inc} show a good agreement with the calculation from the inclusion entrapment conditions, confirming that the α–β transition does not occur at T_c = 847 K in the inclusion.

High-temperature behavior of quartz inclusions in a garnet host

As discussed above, the quartz inclusion does not go through the phase transition near T_c = 847 K because it is under a confining stress. However, if that would be only the effect of increasing hydrostatic pressure, then $\omega(T)$ for A_1(207) and A_1(465) of the inclusion would not have a kink precisely at 847 K, but would rather display the same trends observed for free quartz but shifted to to higher T. Furthermore, while heating from 1000 to 1050 K, the QuiG sample showed rather unexpected and peculiar behavior: it jumped away from the visible field of the microscope through which the laser was focused on the sample, and it was not possible to continue the Raman measurements. Then, the sample was cooled down to room temperature, repositioned, and heated again, but in this second run the sample jumped again and broke into pieces at 1150 K without the quartz going through the α-β phase transition (video ESM_2). After cooling down to room temperature, it was possible to recover only a fragment of the garnet host. The spectra at room temperature for runs 1 and 2 show that the host was not altered by the first heating, whereas the recovered garnet after run 2 has a distinctly different spectrum (Fig. 6b). Consequently, temperature-induced changes in the host can be excluded during the first run. In fact, up to 1000 K the most intense peak of garnet, the A_{1g} mode at ~ 920 cm^{-1}, shows the expected behavior (Fig. 6a), with the peak position decreasing linearly upon heating (Gillet et al 1992). The additional peaks in the spectrum of the recovered garnet from the second run are attributed to nanocrystalline hematite, which forms in almandine upon heating above ~

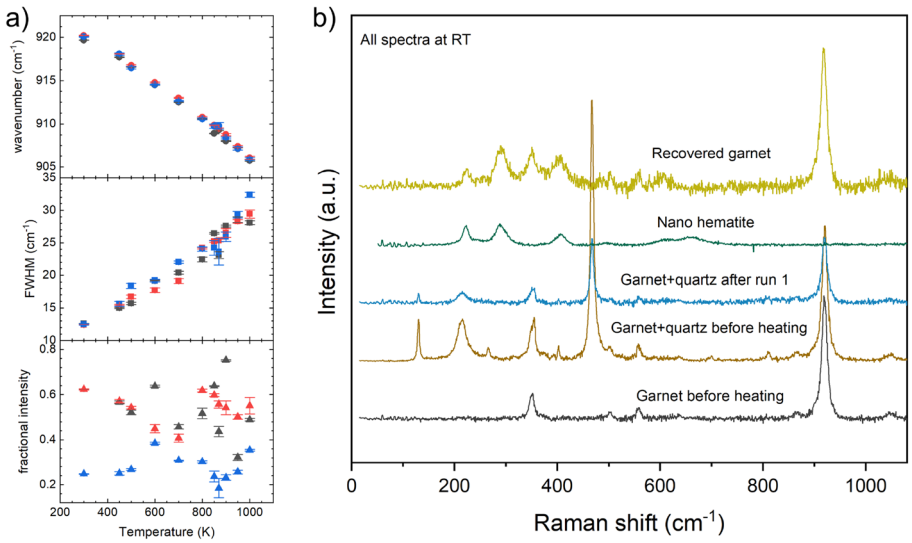

Fig. 6 **a** Temperature dependence of peak positions, widths and fractional intensities of the A_{1g} mode of garnet at ~920 cm^{-1}. Different colors represent spectra collected at the center of the inclusion (blue), on the host-inclusion boundary (red), and away from the inclusion (black). **b** Spectra at room temperature (RT) before run 1 of and run 2 and spectrum of the recovered garnet fragment after run 2. For run 1 two spectra are depicted: at the center of the inclusion and away from the inclusion. A spectrum of nanocrystalline hematite is reported for reference

970 K (Barcova et al 2001; Zboril et al 2004). Additionally, in the spectrum of the recovered fragment, the most intense peak in the garnet host is shifted from 920.05(3) cm^{-1} to 918.07(7) cm^{-1}, reflecting the partial oxidation of Fe^{2+} to Fe^{3+} (Kolesov and Geiger 1998).

Similar macroscopic effects such as jumping have been observed in single crystals and have been called 'dynamic effects' (Naumov et al 2020). In particular, the thermosalient effect is defined as the propensity of a crystal to jump, sometimes to heights of several times its size, when heated over a phase transition, and it is usually accompanied by a large anisotropic change in the unit-cell volume (Skoko et al 2010; Sahoo et al 2013; Panda et al 2014). Jumping has never been reported so far for a host-inclusion system. For example, zircon-in-garnet systems can be heated up to 1400 K (Campomenosi et al 2023), but do not jump or break. This strongly suggests that the elastic anisotropy associated with α-β phase transition is probably the major reason for the occurrence of the thermosalient effect in QuiG. The QuiG system studied here first jumped at 1050 K and then catastrophically broke at 1150 K, that is, well above the ambient-pressure $T_c = 847$ K and right below the calculated $T_c \sim 1167$ K for hydrostatic conditions, suggesting that this peculiar and unexpected behavior is most probably due to the confinement of the quartz grain under anisotropic stress while approaching the α–β phase transition. The energy accumulated in the inclusion due to the hindered phase transition is liberated in the host, causing first the thermosalient effect, the jump, of the whole host-inclusion system and later the mechanical failure of the host.

Conclusions

Our results demonstrate that a quartz inclusion in a garnet host shows a considerably slower expansion than free quartz crystals, since it is under stress due to the confinement by the host garnet. The inclusion stress inferred from the measured Raman shifts of the inclusion are in reasonable agreement with isotropic calculations, at least up to 600 K. Divergence from calculated inclusion pressures at higher temperatures may be due to several effects, including that the hydrostatic calibration of Raman shift in no longer appropriate at higher temperatures as the physical properties of the free quartz change as it approaches the α–β phase transition (as indicated by the strong increase in the FWHM of the soft mode above 600 K, Fig. 2). The stress applied to the quartz inclusion shifts the expected α–β phase transition to higher temperature. As a consequence, the entrapment of the inclusion within the garnet host suppresses the α–β phase transition, which is not observed. Upon further heating, beyond the room-pressure T_c, enormous anisotropic stress is developed at the host-inclusion boundary resulting first in a thermosalient effect of the whole system, and later in the catastrophic shattering of the host mineral. Considering the widespread occurrence of quartz inclusions in crustal rocks, it is possible that the phenomenon of inclusion-triggered cracking of host minerals may have geological consequences on a larger scale.

Supplementary Information The online version contains supplementary material available at https://doi.org/10.1007/s00269-023-01246-5.

Acknowledgements The authors thank Dr. Mattia Gilio for providing the QuiG sample. This work was financially supported by the European Research Council under the European Union's Horizon 2020 research and innovation program grant agreement 714936 (ERC-STG TRUE DEPTHS) to M. Alvaro.

Author contributions All authors contributed to the study conception and design. Material preparation, data collection and analysis were performed by MM, RJA and BM. The first draft of the manuscript was written by Marta Morana and all authors commented on previous versions of the manuscript. All authors read and approved the final manuscript.

Funding Open access funding provided by Università degli Studi di Firenze within the CRUI-CARE Agreement. ERC-STG TRUE DEPTHS grant agreement no. 714936

Data availability Data available within the article or its supplementary materials.

Code availability Not applicable.

Declarations

Conflict of interest The authors declare no conflict of interested.

Ethical approval Not applicable.

Consent to participate Not applicable.

Consent for publication Not applicable.

References

Ackermann RJ, Sorrell CA (1974) Thermal expansion and the high-low transformation in quartz. I. High-temperature X-ray studies. J Appl Crystallogr 7(5):461–467. https://doi.org/10.1107/S0021889874010211

Alvaro M, Mazzucchelli M, Angel R et al (2020) Fossil subduction recorded by quartz from the coesite stability field. Geology 48(1):24–28. https://doi.org/10.1130/G46617.1

Angel RJ, Alvaro M, Miletich R et al (2017) A simple and generalised P-T-V EoS for continuous phase transitions, implemented in EosFit and applied to quartz. Contrib Mineral Petrol 172(5):29. https://doi.org/10.1007/s00410-017-1349-x

Angel RJ, Murri M, Mihailova B et al (2019) Stress, strain and Raman shifts. Z Krist-Cryst Mater 234(2):129–140. https://doi.org/10.1515/zkri-2018-2112

Angel RJ, Gilio M, Mazzucchelli M et al (2022) Garnet EoS: a critical review and synthesis. Contrib Mineral Petrol 177(5):54

Anzolini C, Prencipe M, Alvaro M et al (2018) Depth of formation of super-deep diamonds: Raman barometry of $CaSiO_3$-walstromite inclusions. Am Mineral 103(1):69–74

Ashley KT, Steele-MacInnis M, Bodnar RJ et al (2016) Quartz-in-garnet inclusion barometry under fire: reducing uncertainty from model estimates. Geology 44(9):699–702. https://doi.org/10.1130/G38211.1

Ballato A (2008) Basic material quartz and related innovations. Piezoelectricity. Springer Berlin Heidelberg, Heidelberg, pp 9–35

Barcova K, Mashlan M, Zboril R et al (2001) Thermal decomposition of almandine garnet: Mössbauer study. Czech J Phys 51(7):749–754

Bates JB, Quist AS (1972) Polarized Raman spectra of β-quartz. J Chem Phys 56(4):1528–1533. https://doi.org/10.1063/1.1677402

Bismayer U (1990) Hard mode Raman spectroscopy and its application to ferroelastic and ferroelectric phase transitions. Phase Transit 27(4):211–267

Bonazzi M, Tumiati S, Thomas JB et al (2019) Assessment of the reliability of elastic geobarometry with quartz inclusions. Lithos. https://doi.org/10.1016/j.lithos.2019.105201

Campomenosi N, Mazzucchelli ML, Mihailova B et al (2018) How geometry and anisotropy affect residual strain in host-inclusion systems: coupling experimental and numerical approaches. Am Mineral 103(12):2032–2035. https://doi.org/10.2138/am-2018-6700CCBY

Campomenosi N, Angel RJ, Alvaro M et al (2023) Resetting of zircon inclusions in garnet: Implications for elastic thermobarometry. Geology 51(1):23–27

Carpenter MA, Salje EKH, Graeme-Barber A et al (1998) Calibration of excess thermodynamic properties and elastic constant variations associated with the $\alpha \leftrightarrow \beta$ phase transition in quartz. Am Mineral 83(1):2–22. https://doi.org/10.2138/am-1998-1-201

Cochran W (1960) Crystal stability and the theory of ferroelectricity. Adv Phys 9(36):387–423. https://doi.org/10.1080/00018736000101229

Curie J, Curie P (1880) Développement par compression de l'électricité polaire dans les cristaux hémièdres à faces inclinées. B Mineral 3(4):90–93

Dobrzhinetskaya LF, Eide EA, Larsen RB et al (1995) Microdiamond in high-grade metamorphic rocks of the Western Gneiss region, Norway. Geology 23(7):597–600

Donnay J, Le Page Y (1978) The vicissitudes of the low-quartz crystal setting or the pitfalls of enantiomorphism. Acta Crystallogr A 34(4):584–594

Dove MT, Gambhir M, Heine V (1999) Anatomy of a structural phase transition: theoretical analysis of the displacive phase transition in quartz and other silicates. Phys Chem Miner. https://doi.org/10.1007/s002690050194

Gilio M, Scambelluri M, Angel RJ et al (2022) The contribution of elastic geothermobarometry to the debate on HP versus UHP metamorphism. J Metamorph Geol 40(2):229–242

Gillet P, Fiquetw G, Malezieux JM et al (1992) High-pressure and high-temperature Raman spectroscopy of end-member garnets: pyrope, grossular and andradite. Eur J Miner 4(4):651–664. https://doi.org/10.1127/ejm/4/4/0651

Ginzburg V (1960) Some remarks on phase transitions of the second kind and the microscopic theory of ferroelectric materials [Fiz. Tverd. Tela. 2 2031 (1960)]. Sov Phys-Sol State 1:1824

Glinnemann J, King HE, Schulz H et al (1992) Crystal structures of the low-temperature quartz-type phases of SiO_2 and GeO_2 at elevated pressure. Z Krist-Cryst Mater 198:177–212

Grimm H, Dorner B (1975) On the mechanism of the $\alpha - \beta$ phase transformation of quartz. J Phys Chem Solids 36(5):407–413. https://doi.org/10.1016/0022-3697(75)90066-9

Hazen RM, Finger LW, Hemley RJ et al (1989) High-pressure crystal chemistry and amorphization of α-quartz. Solid State Commun 72(5):507–511. https://doi.org/10.1016/0038-1098(89)90607-8

Heine V, Welche PR, Dove MT (1999) Geometrical origin and theory of negative thermal expansion in framework structures. J Am Ceram Soc 82(7):1793–1802

Jorgensen JD (1978) Compression mechanisms in α-quartz structures-SiO_2 and GeO_2. J Appl Phys 49(11):5473–5478. https://doi.org/10.1063/1.324517

Kolesov BA, Geiger CA (1998) Raman spectra of silicate garnets. Phys Chem Miner 25(2):142–151. https://doi.org/10.1007/s002690050097

Kuzmany H (2009) Solid-state spectroscopy: an introduction. Springer Berlin Heidelberg, Heidelberg

Larsen RB, Eide EA, Burke EA (1998) Evolution of metamorphic volatiles during exhumation of microdiamond-bearing granulites in the Western Gneiss Region, Norway. Contrib Mineral Petrol 133(1–2):106–121

Liu P, Massonne HJ (2019) An anticlockwise P-T-t path at high-pressure, high-temperature conditions for a migmatitic gneiss from the island of fjørtoft, Western Gneiss Region, Norway, indicates two burial events during the Caledonian orogeny. J Metamorph Geol 37(4):567–588

Mazzucchelli ML, Burnley P, Angel RJ et al (2018) Elastic geothermobarometry: corrections for the geometry of the host-inclusion system. Geology 46(3):231–234. https://doi.org/10.1130/G39807.1

Mazzucchelli ML, Angel RJ, Alvaro M (2021) Entrapt: an online platform for elastic geothermobarometry. Am Mineral 106(5):830–837

Morana M, Mihailova B, Angel RJ et al (2020) Quartz metastability at high pressure: what new can we learn from polarized Raman spectroscopy? Phys Chem Miner 47(8):34. https://doi.org/10.1007/s00269-020-01100-y

Murri M, Mazzucchelli ML, Campomenosi N et al (2018) Raman elastic geobarometry for anisotropic mineral inclusions. Am Mineral 103(11):1869–1872. https://doi.org/10.2138/am-2018-6625CCBY

Murri M, Alvaro M, Angel RJ et al (2019) The effects of non-hydrostatic stress on the structure and properties of alpha-quartz. Phys Chem Miner. https://doi.org/10.1007/s00269-018-01018-6

Naumov P, Karothu DP, Ahmed E et al (2020) The rise of the dynamic crystals. J Am Chem Soc 142(31):13256–13272. https://doi.org/10.1021/jacs.0c05440

Panda MK, Runcevski T, Sahoo SC et al (2014) Colossal positive and negative thermal expansion and thermosalient effect in a pentamorphic organometallic martensite. Nat Commun 5(1):1–8

Raman CV, Nedungadi TMK (1940) The $\alpha - \beta$ transformation of quartz. Nature 145(3665):147. https://doi.org/10.1038/145147a0

Sahoo SC, Panda MK, Nath NK et al (2013) Biomimetic crystalline actuators: structure-kinematic aspects of the self-actuation and motility of thermosalient crystals. J Am Chem Soc 135(33):12241–12251

Salje EKH, Ridgwell A, Guttler B et al (1992) On the displacive character of the phase transition in quartz: a hard-mode spectroscopy study. J Phys-Condens Mat 4(2):571–577

Scheidl KS, Kurnosov A, Trots DM et al (2016) Extending the single-crystal quartz pressure gauge up to hydrostatic pressure of 19 GPa. J Appl Crystallogr 49(6):2129–2137. https://doi.org/10.1107/S1600576716015351

Schmidt C, Ziemann MA (2000) In-situ Raman spectroscopy of quartz: a pressure sensor for hydrothermal diamond-anvil cell experiments at elevated temperatures. Am Mineral 85(11):1725–1734. https://doi.org/10.2138/am-2000-11-1216

Scott JF (1968) Evidence of coupling between one- and two-phonon excitations in quartz. Phys Rev Lett 21(13):907–910. https://doi.org/10.1103/PhysRevLett.21.907

Scott JF (1974) Soft-mode spectroscopy: experimental studies of structural phase transitions. Rev Mod Phys 46(1):83–128. https://doi.org/10.1103/RevModPhys.46.83

Shen AH, Bassett WA, Chou IM (1993) The $\alpha - \beta$quartz transition at high temperatures and pressures in a diamond-anvil cell by laser interferometry. Am Mineral 78(7):694–698

Skoko Z, Zamir S, Naumov P et al (2010) The thermosalient phenomenon. "Jumping crystals" and crystal chemistry of the anticholinergic agent oxitropium bromide. J Am Chem Soc 132(40):14191–14202

Wang J, Mao Z, Jiang F et al (2015) Elasticity of single-crystal quartz to 10 GPa. Phys Chem Miner 42(3):203–212. https://doi.org/10.1007/s00269-014-0711-z

Welche P, Heine V, Dove M (1998) Negative thermal expansion in beta-quartz. Phys Chem Miner 26:63–77

Zboril R, Mashlan M, Machala L et al (2004) Characterization and thermal behaviour of garnets from almandine-pyrope series at 1200°c. Hyperfine Interact 156(157):403–410. https://doi.org/10.1007/978-1-4020-2852-6_61